



**HAL**  
open science

# Mechanistic Study of Cast and 3D-Printed Stainless Steel Electropolishing in Acid Media and Deep Eutectic Solvents

Chloé Rotty, Marie-Laure Doche, Audrey Mandroyan, Vincent Vivier,  
Jean-Yves Hihn

► **To cite this version:**

Chloé Rotty, Marie-Laure Doche, Audrey Mandroyan, Vincent Vivier, Jean-Yves Hihn. Mechanistic Study of Cast and 3D-Printed Stainless Steel Electropolishing in Acid Media and Deep Eutectic Solvents. *Journal of The Electrochemical Society*, 2022, 169 (7), pp.071504. 10.1149/1945-7111/ac7bb3 . hal-04294211

**HAL Id: hal-04294211**

**<https://hal.science/hal-04294211v1>**

Submitted on 19 Nov 2023

**HAL** is a multi-disciplinary open access archive for the deposit and dissemination of scientific research documents, whether they are published or not. The documents may come from teaching and research institutions in France or abroad, or from public or private research centers.

L'archive ouverte pluridisciplinaire **HAL**, est destinée au dépôt et à la diffusion de documents scientifiques de niveau recherche, publiés ou non, émanant des établissements d'enseignement et de recherche français ou étrangers, des laboratoires publics ou privés.

1 Mechanistic study of cast and 3D-printed stainless steel  
2 electropolishing in acid media and deep eutectic solvents

3 Chloé Rotty<sup>a</sup>, Marie-Laure Doche<sup>a</sup>, Audrey Mandroyan<sup>a</sup>, Vincent Vivier<sup>b,\*</sup>,  
4 Jean-Yves Hihn<sup>a,\*\*</sup>

5 <sup>a</sup>*Institut UTINAM, UMR CNRS 6213, Université de Bourgogne Franche-Comté, 30*  
6 *avenue de l'Observatoire, 25 009 Besançon, France*

7 <sup>b</sup>*Sorbonne Université, CNRS, Laboratoire de Réactivité de Surface, 4 place Jussieu,*  
8 *75005, Paris, France*

---

9 **Abstract**

The mechanistic analysis of the electropolishing procedure of stainless steel (SS) was revisited using electrochemical impedance spectroscopy. Firstly, the control of the dissolution reaction by diffusion was confirmed with the linear dependence of the limiting current density as a function of the electrode rotation rate using the Levich's law. Nevertheless, varying the viscosity (by changing temperature from 35°C to 70°C) show a direct relationship between the diffusion coefficient and the kinematic viscosity, irrespective of the cation concentration at the interface, thus suggesting a minor role in the diffusion limiting step. This limitation is therefore provided by the diffusion of an acceptor specie from the electrolyte toward the anode surface. To discriminate the role of water or mineral anion in the so-called acceptor model, a full descriptive model of the electrochemical behaviour of interface was devised for analyzing electropolishing results obtained by electrochemical impedance spectroscopy (EIS) for both cast and additive layer manufacturing (ALM) 316L SS in aqueous acid electrolyte and in deep eutectic solvent (DES). It was shown that the model involving an acceptor specie allows to describe with a good accuracy the electrochemical behavior of the different systems at several potentials.

10 *Keywords:* Electrochemical impedance spectroscopy, Ionic liquid,  
11 Electrochemical dissolution, Surface treatment, Additive manufacturing

---

\*vincent.vivier@sorbonne-universite.fr (Vincent Vivier)

\*\*jean-yves.hihn@univ-fcomte.fr (Jean-Yves Hihn)

## 12 1. Introduction

13 Over the last decades, innovative manufacturing processes [1, 2, 3] has  
14 emerged, enabling the production of metal workpieces with both complex  
15 shapes and sophisticated internal structures such as fluid flow channels [4].  
16 Among all the available techniques, Additive Layer Manufacturing (ALM)  
17 and more specifically Selective Laser Melting (SLM) consists in fabricating  
18 3-dimensional objects by successively adding material layer by layer [5, 6].  
19 These manufacturing processes are a complete break with conventional ones  
20 based on a subtractive approach such as machining. Typical SLM processes  
21 can be considered as fast solidification processes during which temperature  
22 gradients generate complex macro and microstructures [7]. Moreover, the  
23 surface appearance of the metal workpieces may be indeed of poor quality  
24 (depending on metallic powder characteristics) compared to that obtained  
25 when the workpieces come out of machining. The direct use of additive  
26 manufacturing parts without a finishing stage is therefore often not possible,  
27 which requires the implementation of a subsequent surface treatment step.

28 Electropolishing (EP) process is now extensively considered as post-  
29 traitement particularly for additive manufacturing parts. This wet elec-  
30 trolytic process consists in a controlled dissolution of metallic surfaces lead-  
31 ing to a decrease of the surface roughness which is usually accompanied by a  
32 brightness increase [8, 9]. Unlike the other mechanical polishing techniques,  
33 EP process does not induce any residual stresses since the metal layers on  
34 the surface are not hardened, but softly removed by electrochemical dissolu-  
35 tion. The main problem in carrying out this oxidation reaction is to deter-  
36 mine the most suitable electrolyte composition and experimental conditions.  
37 Although this process is usually carried out in concentrated acidic media,  
38 alternative environmentally-friendly electrolytes have been developed in re-  
39 cent years such as Deep Eutectic Solvents (DESs) [10, 11, 12] or in sulfuric  
40 acid free electrolyte [13], depending on the type of metal.

41 It has already been reported in several papers that three to four dis-  
42 tinct regions can be seen on a typical electropolishing polarization curve  
43 [14, 15, 16]. Starting from the corrosion potential and moving towards more  
44 anodic potentials, the first domain is ascribed to active dissolution of the

45 substrate after oxide layer breakdown. The second region refers to a vis-  
46 cous film formation at the electrolyte/substrate interface, but is not always  
47 seen on the current/potential curve. The third region is the limiting cur-  
48 rent plateau and is characteristic of a diffusion controlled mechanism: this  
49 is the electropolishing zone. The fourth region for the higher overpotential,  
50 corresponds to solvent oxidation and oxygen evolution reactions.

51 Studies have shown that levelling can be carried out under primary cur-  
52 rent distribution (i.e., controlled by ohmic drop), secondary current distribu-  
53 tion (controlled by charge transfer considering that concentration gradient  
54 are negligible) and tertiary current distribution (controlled by mass trans-  
55 fer) [17, 18, 19]. Brightening is only possible when dissolution is limited by  
56 mass transfer and when a homogeneous layer covers the surface. It should  
57 be noticed that these EP description and analysis were mainly developed to  
58 account for the profile shape of the material surface and the geometry of the  
59 electrochemical cell, independently of the dissolution mechanism itself.

60 Following the seminal works of Jacquet [20, 21], Elmore [22, 23] and  
61 Wagner [24], Edwards [25, 26] developed a model accounting for an acceptor  
62 species such as anion or solvent molecules that complex the metal cation, thus  
63 controlling the rate of the dissolution. Matloz [27] developed the mathemat-  
64 ical expression of the electrochemical impedance accounting for the physical  
65 bases for salt film and acceptor models. This general description provided a  
66 first approach for the mechanistic analysis based on the analysis of the shape  
67 of the Nyquist diagrams, but the electrochemical reaction was described as  
68 simple charge transfer reaction, neglecting possible formation of adsorbate  
69 nor taking into account more complex chemical steps.

70 Based on steady-state and EIS measurements, Bojinov et al. introduced  
71 a kinetic model for describing the passivation mechanism of iron in con-  
72 centrated phosphoric solution [28]. Interestingly, this mechanism involves  
73 surface intermediates leading to the formation of Fe(II) and Fe(III), whereas  
74 the formation of Fe(I) was assumed to be negligible. Conversely, using elec-  
75 trohydrodynamic impedance for a fine investigation of the mass transfer  
76 contribution mechanism in sulphuric acid solution, Barcia et al. developed  
77 a model accounting for the formation of a thin film with a viscosity profile  
78 spreading from the electrode surface to the bulk solution, which also involves

79 monovalent and divalent Fe intermediates [29]. Additionally, one can expect  
80 different time constants in the EIS response depending on the metal and the  
81 electrolyte.

82 Given the complexity of the electropolishing process, many mechanisms  
83 have also been proposed for steel. In this respect, this work focuses on the  
84 electropolishing mechanism, which has been investigated by Linear Sweep  
85 Voltammetry (LSV) and Electrochemical Impedance Spectroscopy (EIS) for  
86 cast and ALM 316L Stainless Steel in both concentrated phosphoric and  
87 sulphuric acid media and choline chloride-ethylene glycol mixtures. To dis-  
88 criminate the role of water or mineral anion, a full descriptive model of the  
89 electrochemical behaviour of interface was developed. This model found its  
90 roots in iron dissolution and electropolishing considerations. EIS measure-  
91 ments were carried out in acidic and DES media in order to confront exper-  
92 imental results with the simulations of the dissolution reaction. In the first  
93 case, water was assumed to be the limiting specie and in the second case an  
94 acceptor specie (such as phosphates or chlorides) was considered. The same  
95 study has been performed for both cast and additive manufacturing 316L  
96 Stainless Steel. In all cases, the proposed model allows to describe with a  
97 good accuracy the electrochemical behaviour of the EP process at different  
98 potentials.

## 99 2. Experimental

100 The working electrodes consisted of a 316L stainless steel disk electrodes  
101 of 3.5 mm in diameter ( $9.62 \text{ mm}^2$ ) of both cast or additive layer manufac-  
102 turing metals, the compositions of which are given in Table 1. Before each  
103 experiment, the electrode surface was mechanically polished with abrasive  
104 SiC paper (P1200), rinsed with alcohol and dried with compressed air. Then,  
105 the material was mounted on a rotating-disk electrode (RDE).

Table 1: Elemental composition of the alloys

Composition (wt.%)	Fe	Cr	Ni	Mo	Mn
Cast 316L	67.7	17.3	11.4	2.1	1.5
ALM 316L	66.8	17.4	11.7	3.9	0.1

106 The electrolyte solutions consisted of either a mixture of 45% H<sub>3</sub>PO<sub>4</sub>,  
 107 35% H<sub>2</sub>SO<sub>4</sub> and 20% H<sub>2</sub>O or a choline chloride (ChCl) + ethylene glycol  
 108 (EG) in a molar ratio (1:2). The physicochemical properties of both solvents  
 109 used in this work are presented in Table 2. Electrochemical experiments were  
 110 carried out in a jacketed glass reactor for controlling the temperature within  
 111 a 3-electrode configuration. The electrolyte temperature was regulated at 70  
 112  $\pm 1^\circ\text{C}$  and the volume of electrolyte for each experiment was 200 mL. The  
 113 electrochemical experiments (polarization curves, electrochemical impedance  
 114 spectroscopy diagrams) were performed with a SP 240 potentiostat (Bio-  
 115 Logic). The counter and reference electrodes were a large area platinized  
 116 titanium grid facing the working electrode and a saturated calomel reference  
 117 electrode ( $E_{SCE} = 0.241 \text{ V/SHE}$ ), respectively. EP procedure was carried  
 118 out under a potentiostatic control at different potentials. Each EIS measure-  
 119 ment was performed after the polarization of the sample for 1 minute. The  
 120 frequency domain investigated was 1 MHz down to 100 mHz, with 10 points  
 121 per decade of frequency and a sine wave amplitude of 10 mV<sub>rms</sub>.

Table 2: Physicochemical properties of the solvents used for the electropolishing procedure

	T / °C	$\rho$ / g cm <sup>-3</sup>	$\eta$ / mPa s	$\sigma$ / mS cm <sup>-1</sup>
45% H <sub>3</sub> PO <sub>4</sub> + 35% H <sub>2</sub> SO <sub>4</sub> + 20% H <sub>2</sub> O	25	1.56	6.88	178.3
	70	1.548	2.79	324.9
ChCl + EG (1:2)	25	1.116	31.35	9.04
	70	1.097	7.88	30.05

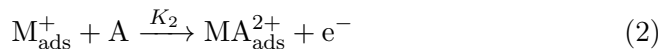
### 122 3. Models for the electropolishing

#### 123 3.1. Model

124 In this work, electrochemical polishing is described by successive elemen-  
 125 tal one-electron reactions as previously done for the study of the dissolution  
 126 mechanism of different metals [30, 31, 32, 33], M, and accounting for the  
 127 formation of adsorbed species as reaction intermediates.



128



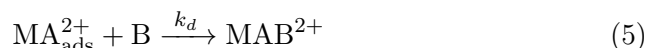
129 in which A is a species used to complex metal cations, and  $K_1$  and  $K_2$  are  
 130 the reaction rates of the electrochemical reactions which are exponentially  
 131 potential dependent (Tafel's law) and express as

$$K_1 = k_1 e^{\left(\frac{\alpha_1 F}{RT} E\right)} \quad (3)$$

132

$$K_2 = k_2 e^{\left(\frac{\alpha_2 F}{RT} E\right)} \quad (4)$$

133 where  $E$  is the electrode potential (in V),  $k_1$  and  $k_2$  are the potential in-  
 134 dependent reaction rates of each step,  $\alpha_1$  and  $\alpha_2$  are the charge transfer  
 135 coefficients, and  $F$ ,  $R$ , and  $T$  are the Faraday constant (96485 C mol<sup>-1</sup>), the  
 136 gas constant (8.314 J K<sup>-1</sup> mol<sup>-1</sup>), and the temperature (in K), respectively.  
 137 It is also interesting to note that this mechanism involves the dissolution of  
 138 metals in the form of divalent ions, i.e. we assume that the chromium in the  
 139 steel contributes little or nothing to the impedance response. Additionally,  
 140 we assume that the adsorption isotherms corresponding to the formation /  
 141 consumption of reaction intermediates  $M_{\text{ads}}^+$  and  $MA_{\text{ads}}^{2+}$  obey a Langmuir  
 142 isotherm and are characterized by the surface coverages  $\theta_1$  and  $\theta_2$ , respec-  
 143 tively. The last step is the dissolution of the adsorbed complex formed at  
 144 the electrode surface,  $MA_{\text{ads}}^{2+}$ , which can be expressed as



145 where  $k_d$  is the kinetic constant of the chemical reaction, and B a species,  
 146 such as a water molecule, which promotes the dissolution of the metal com-  
 147 plex  $MA_{\text{ads}}^{2+}$ . At this point, it is interesting to mention that the species A  
 148 is considered to be the acceptor species for complexing the metal cations  
 149 (*i.e.* phosphate type species) and species B is considered to be the water  
 150 molecules contained in the solvent, but in both cases, the concentrations of  
 151 A and B at the electrode surface are controlled by diffusion. As previously  
 152 described in the literature, two hypotheses can be formulated a priori con-  
 153 cerning the nature of the limiting step in the EP process: either A or B is  
 154 the limiting species, but in both cases the concentration of the other species  
 155 remains constant at the electrode surface.

156 *3.2. Derivation of the impedance expression*

157 The rates of the 3 reactions (1),(2), and (5) are given by

$$v_1 = K_1 (1 - \theta_1 - \theta_2) \quad (6)$$

$$v_2 = K_2 [A]_0 \theta_1 \quad (7)$$

$$v_3 = k_d [B]_0 \theta_2 \quad (8)$$

158 The time evolution relationship for surface coverages express as

$$\beta \frac{d\theta_1}{dt} = v_1 - v_2 = K_1 (1 - \theta_1 - \theta_2) - K_2 [A]_0 \theta_1 \quad (9)$$

159

$$\beta \frac{d\theta_2}{dt} = v_2 - v_3 = K_2 [A]_0 \theta_1 - k_d [B]_0 \theta_2 \quad (10)$$

160 where  $\beta$  is the surface concentration for complete coverage (in mol cm<sup>-2</sup>).

161 At steady-state, the surface coverage for each species is constant, and thus

$$\frac{d\theta_1}{dt} = 0 \quad (11)$$

162 and

$$\frac{d\theta_2}{dt} = 0 \quad (12)$$

163 leading to the set of equations

$$\begin{cases} K_1 (1 - \theta_1 - \theta_2) - K_2 [A]_0 \theta_1 = 0 \\ K_2 [A]_0 \theta_1 - k_d [B]_0 \theta_2 = 0 \end{cases} \quad (13)$$

164 allowing the steady-state surface coverages,  $\bar{\theta}_1$  and  $\bar{\theta}_2$ , to be expressed as

$$\bar{\theta}_1 = \frac{K_1 k_d [B]_0}{K_1 k_d [B]_0 + K_1 K_2 [A]_0 + K_2 [A]_0 k_d [B]_0} \quad (14)$$

165

$$\bar{\theta}_2 = \frac{K_1 K_2 [A]_0}{K_1 k_d [B]_0 + K_1 K_2 [A]_0 + K_2 [A]_0 k_d [B]_0} \quad (15)$$

166 where  $[A]_0$  and  $[B]_0$  are the concentration of  $A$  and  $B$  at the electrode surface,  
167 respectively.

168 The faradaic current is given by the algebraic sum of each electrochemical  
169 contribution (on the anodic domain, the cathodic contribution to the current  
170 was neglected)

$$i = F (v_1 + v_2) \quad (16)$$

171

$$i = F [K_1 (1 - \theta_1 - \theta_2) + K_2 [A]_0 \theta_1] \quad (17)$$

172 thus allowing the equation of the steady-state polarization curve to be de-  
173 rived

$$i = F [K_1 (1 - \bar{\theta}_1 - \bar{\theta}_2) + K_2 [A]_0 \bar{\theta}_1] \quad (18)$$

174 The faradaic impedance,  $Z_f$ , is obtained from the first order of the Taylor  
175 expansion of the current, which can be expressed in the Laplace domain as

$$\begin{aligned} \frac{1}{Z_f(p)} = \frac{\Delta i(p)}{\Delta E(p)} &= \left( \frac{\partial i}{\partial E} \right)_{\theta_1, \theta_2, [A]_0} + \left( \frac{\partial i}{\partial \theta_1} \right)_{E, \theta_2, [A]_0} \frac{\Delta \theta_1(p)}{\Delta E(p)} \\ &+ \left( \frac{\partial i}{\partial \theta_2} \right)_{E, \theta_1, [A]_0} \frac{\Delta \theta_2(p)}{\Delta E(p)} + \left( \frac{\partial i}{\partial [A]_0} \right)_{E, \theta_1, \theta_2} \frac{\Delta [A]_0(p)}{\Delta E(p)} \end{aligned} \quad (19)$$

176 where  $p$  is the variable in the Laplace domain  $p \equiv j\omega$ , where  $j = \sqrt{-1}$ ,  $\omega$  is  
177 the angular frequency ( $\omega = 2\pi f$ ), and  $f$  the frequency in Hz. Each partial  
178 derivative can then be evaluated a function of the model parameters as

$$\left( \frac{\partial i}{\partial E} \right)_{\theta_1, \theta_2, [A]_0} = F \left[ \frac{\alpha_1 F}{RT} K_1 (1 - \theta_1 - \theta_2) + \frac{\alpha_2 F}{RT} K_2 [A]_0 \theta_1 \right] \quad (20)$$

179

$$\left( \frac{\partial i}{\partial \theta_1} \right)_{E, \theta_2, [A]_0} = F (K_2 [A]_0 - K_1) \quad (21)$$

180

$$\left( \frac{\partial i}{\partial \theta_2} \right)_{E, \theta_1, [A]_0} = -F K_1 \quad (22)$$

181

$$\left( \frac{\partial i}{\partial [A]_0} \right)_{E, \theta_1, \theta_2} = F K_2 \theta_1 \quad (23)$$

182 Additionally, from the linearization of Eqs.(9) and (10) it comes

$$\begin{aligned} j\omega\beta\Delta\theta_1 &= \left[ \frac{\alpha_1 F}{RT} K_1 (1 - \theta_1 - \theta_2) - \frac{\alpha_2 F}{RT} K_2 [A]_0 \theta_1 \right] \Delta E \\ &- (K_1 + K_2 [A]_0) \Delta\theta_1 - K_1 \Delta\theta_2 - K_2 \theta_1 \Delta [A]_0 \end{aligned} \quad (24)$$

183

$$\begin{aligned} j\omega\beta\Delta\theta_2 &= \frac{\alpha_2 F}{RT} K_2 [A]_0 \theta_1 \Delta E + K_2 [A]_0 \Delta\theta_1 - k_d [B]_0 \Delta\theta_2 \\ &- k_d \theta_2 \Delta [B]_0 + K_2 \theta_1 \Delta [A]_0 \end{aligned} \quad (25)$$

184 For sake of simplicity, the thickness of the diffusion layer,  $\delta$ , for both diffusing  
185 species, is expressed as

$$\delta = 1.61 D_s^{1/3} \Omega^{-1/2} \nu^{1/6} \quad (26)$$

186 where  $D_s$  is the diffusion coefficient of the species  $s$  (in  $\text{cm}^2 \text{s}^{-1}$ ),  $\Omega$  the  
 187 rotation rate of the RDE (in  $\text{rad s}^{-1}$ ), and  $\nu$  the kinematic viscosity (in  $\text{cm}^2$   
 188  $\text{s}^{-1}$ ). The concentration of diffusing species can be obtained from the solution  
 189 of the second Fick's law under the assumption of diffusion through a film  
 190 with exchange of electroactive species between the film and the electrolyte  
 191 (transmissive boundary condition) [34, 35].

$$\frac{\Delta [A]_0}{\Delta i} = \frac{1}{FD_A} \frac{\tanh\left(\delta\sqrt{\frac{j\omega}{D_A}}\right)}{\sqrt{\frac{j\omega}{D_A}}} \quad (27)$$

192

$$\frac{\Delta [B]_0}{\Delta i} = \frac{1}{FD_B} \frac{\tanh\left(\delta\sqrt{\frac{j\omega}{D_B}}\right)}{\sqrt{\frac{j\omega}{D_B}}} \quad (28)$$

193 It is worth mentioning that A and B do not play a symmetrical role in the  
 194 EP mechanism as shown by Eqs. (1), (2), and (5), and thus at this point,  
 195 two cases have to be envisioned for the derivation of the analytical expression  
 196 of the impedance: either B is the limiting species and it is assumed that the  
 197 concentration of A remains constant in the whole electrolyte, including at  
 198 the electrode surface, either A is the limiting species and it is assumed that  
 199 the concentration of B remains constant in the electrolyte.

### 200 3.2.1. B is the limiting species

201 Assuming that B is the limiting species, Eq.(28) expresses as

$$\frac{\Delta [B]_0}{\Delta E} = \frac{1}{Z_f} \frac{1}{FD_B} \frac{\tanh\left(\delta\sqrt{\frac{j\omega}{D_B}}\right)}{\sqrt{\frac{j\omega}{D_B}}} \quad (29)$$

202 and Eqs.(19), (24) and (25) can be written as linear system of equations

$$\left\{ \begin{array}{l} (j\omega\beta + K_1 + K_2 [A]_0) \frac{\Delta\theta_1}{\Delta E} + K_1 \frac{\Delta\theta_2}{\Delta E} = \\ \quad \left[ \frac{\alpha_1 F}{RT} K_1 (1 - \theta_1 - \theta_2) - \frac{\alpha_2 F}{RT} K_2 [A]_0 \theta_1 \right] \\ -K_2 [A]_0 \frac{\Delta\theta_1}{\Delta E} + (j\omega\beta + k_d [B]_0) \frac{\Delta\theta_2}{\Delta E} + \frac{k_d \theta_2}{FD_B} \frac{\tanh\left(\delta\sqrt{\frac{j\omega}{D_B}}\right)}{\sqrt{\frac{j\omega}{D_B}}} \frac{1}{Z_f F} = \\ \quad \frac{\alpha_2 F}{RT} K_2 [A]_0 \theta_1 \\ F (K_1 - K_2 [A]_0) \frac{\Delta\theta_1}{\Delta E} + F K_1 \frac{\Delta\theta_2}{\Delta E} + \frac{1}{Z_f F} = \\ \quad F \left[ \frac{\alpha_1 F}{RT} K_1 (1 - \theta_1 - \theta_2) + \frac{\alpha_2 F}{RT} K_2 [A]_0 \theta_1 \right] \end{array} \right. \quad (30)$$

203 The faradaic impedance is then obtain as a solution of this system of 3  
 204 linear equations.

205 3.2.2. *A is the limiting species*

206 Assuming that A is the limiting species, Eq.(27) expresses as

$$\frac{\Delta [A]_0}{\Delta E} = \frac{1}{Z_f} \frac{1}{FD_A} \frac{\tanh\left(\delta\sqrt{\frac{j\omega}{D_A}}\right)}{\sqrt{\frac{j\omega}{D_A}}} \quad (31)$$

207 and Eqs.(19), (24) and (25) can be written as linear system of equations

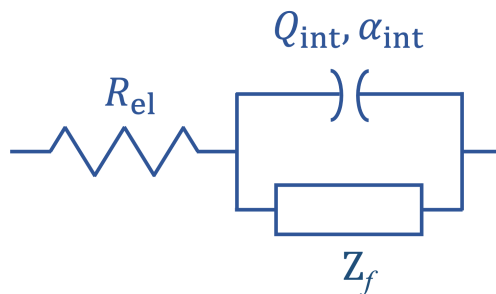
$$\left\{ \begin{array}{l} (j\omega\beta + K_1 + K_2 [A]_0) \frac{\Delta\theta_1}{\Delta E} + K_1 \frac{\Delta\theta_2}{\Delta E} + \frac{K_2\theta_1}{FD_A} \frac{\tanh\left(\delta\sqrt{\frac{j\omega}{D_A}}\right)}{\sqrt{\frac{j\omega}{D_A}}} \frac{1}{Z_f F} = \\ \quad \left[ \frac{\alpha_1 F}{RT} K_1 (1 - \theta_1 - \theta_2) - \frac{\alpha_2 F}{RT} K_2 [A]_0 \theta_1 \right] \\ -K_2 [A]_0 \frac{\Delta\theta_1}{\Delta E} + (j\omega\beta + k_d [B]_0) \frac{\Delta\theta_2}{\Delta E} - \frac{K_2\theta_1}{FD_A} \frac{\tanh\left(\delta\sqrt{\frac{j\omega}{D_A}}\right)}{\sqrt{\frac{j\omega}{D_A}}} \frac{1}{Z_f F} = \\ \quad \frac{\alpha_2 F}{RT} K_2 [A]_0 \theta_1 \\ F (K_1 - K_2 [A]_0) \frac{\Delta\theta_1}{\Delta E} + F K_1 \frac{\Delta\theta_2}{\Delta E} + \left( 1 - F \frac{K_2\theta_1}{FD_A} \frac{\tanh\left(\delta\sqrt{\frac{j\omega}{D_A}}\right)}{\sqrt{\frac{j\omega}{D_A}}} \right) \frac{1}{Z_f F} = \\ \quad F \left[ \frac{\alpha_1 F}{RT} K_1 (1 - \theta_1 - \theta_2) + \frac{\alpha_2 F}{RT} K_2 [A]_0 \theta_1 \right] \end{array} \right. \quad (32)$$

208 The faradaic impedance is then obtain as a solution of this system of 3  
209 linear equations.

210 3.3. *Parameters for the modelling*

211 The fit of the parameters was performed using both Levenberg-Marquardt  
212 and step-by-step simplex regressions implemented in the measurement model  
213 tool developed by Orazem group.[36] Whatever the model considered, the  
214 number of parameters involved in the model is large. It is worth mention-  
215 ing that the use of electrical equivalent circuit should also have resulted in  
216 a large number of parameters, with the added difficulty that it would then  
217 be very difficult to express any link between these parameters. However, a  
218 careful inspection of both systems of equations shows that some parameters  
219 are correlated. For the first step, it is not possible to determine indepen-  
220 dently  $K_1$  and  $\alpha_1$ , but one can only access to the product  $K_1\alpha_1$ . Similarly,  
221 for the second electrochemical step, it is not possible to determine  $K_2$ ,  $\alpha_1$   
222 and  $\alpha_2$ , one can only get  $K_2(\alpha_1 + \alpha_2)$ , whereas for the chemical reaction,  
223 we can determine  $K_d [B]_0$ . Then for a global fitting of the experimental re-  
224 sults, an interfacial capacitance (or a constant phase element,  $Q_{int}$ ,  $\alpha_{int}$ ) has

225 to be added in parallel to the faradaic impedance,  $Z_f$ , as shown in Fig.1,  
 226 together with the electrolyte resistance,  $R_{el}$ , in series. The electrolyte resis-  
 227 tance was evaluated via the measurements model,[37] the other parameters  
 228 or a combination of them were left free for the fitting procedure.



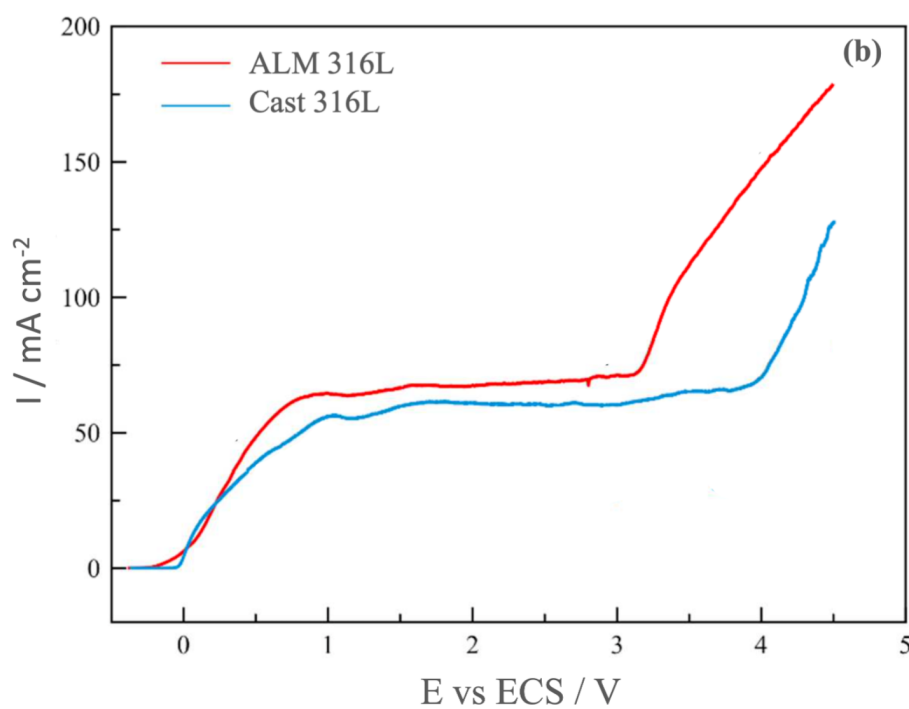
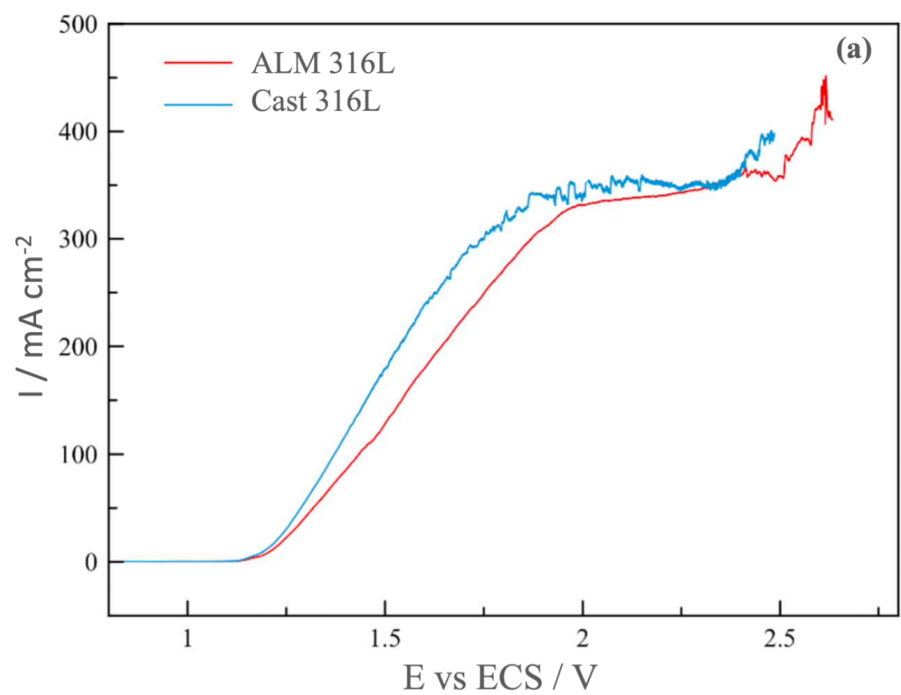
229

Figure 1: Electrical equivalent circuit used to analyse the EIS spectra.  $Z_f$  allows to intro-  
 230 duce the analytical expression of the impedance that is derived from the electropolishing  
 model presented in this work.

#### 231 4. Results and discussion

232 Fig. 2 shows the anodic polarization curves of cast and ALM 316L per-  
 233 formed at  $2 \text{ mV s}^{-1}$  in sulfuric acid solution (Fig. 2a) and in ChCl-EG (1:2)  
 234 (Fig. 2b) at  $70^\circ\text{C}$ . Interestingly, the global shape of the curves in acidic so-  
 235 lution and in DES are similar, only the current density and the length of  
 236 the current plateau vary. Moreover, for both materials, curves remain un-  
 237 changed in shape and allow to define 3 regions: the first one corresponds to  
 238 the current increase and is ascribed to the active domain (dissolution of the  
 239 alloys). The linear shape of the curves during the rise of the current when the  
 240 potential increases is due to the uncompensated contribution of the ohmic  
 241 drop (raw data without any compensation are presented in this figure). The  
 242 second domain is a current plateau that spreads over 500 mV due to diffu-  
 243 sion limited current. The last domain is characterized by a second increase  
 244 in current, which is ascribed to the solvent and oxygen oxidation reactions.  
 245 A first rough analysis of the experimental results therefore allows the con-  
 246 clusion that both alloys seems to follow a similar electrochemical behavior  
 247 in the different electrolytes but with a shorter current plateau in acidic so-  
 248 lutions than in DES. Moreover, the EP process that is usually performed at

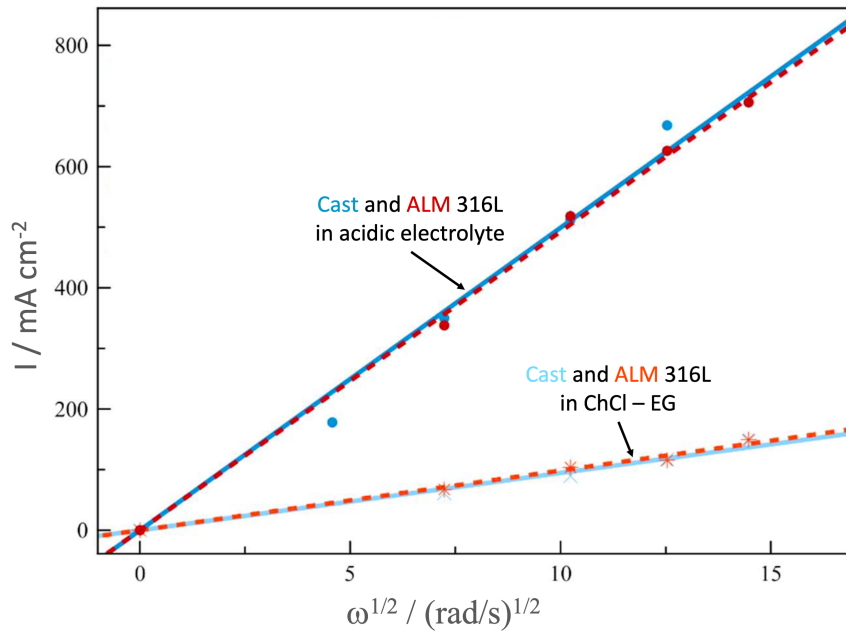
249 a potential corresponding to the limiting current indicates that the global  
250 EP kinetics are similar for both materials. Additionally, the control of the  
251 dissolution reaction by diffusion was confirmed with the linear dependence  
252 of the limiting current density as a function of the electrode rotation rate as  
253 described by the Levich's law, as shown on Fig. 3. The limiting current is  
254 comparable for Cast and ALM materials and follows the same trend what-  
255 ever the rotation rate and the media (DES and acidic solution). Moreover,  
256 in acidic media, varying the viscosity e.g. by changing temperature from  
257 35°C to 70°C, shows a direct relationship between the diffusion coefficient  
258 and the kinematic viscosity, irrespective of the cation concentration at the  
259 interface, which suggest a minor role in the diffusion limiting step [19, 27].  
260 This limitation is therefore ascribed to the diffusion of an acceptor species  
261 from the electrolyte toward the anode surface.



262

Figure 2: Polarization curves obtained for cast and ALM 316L at  $2 \text{ mV s}^{-1}$  and  $\Omega = 500$  rpm in acidic mixture (a) and in ChCl-EG (1:2) at  $70^\circ\text{C}$  (b)

263

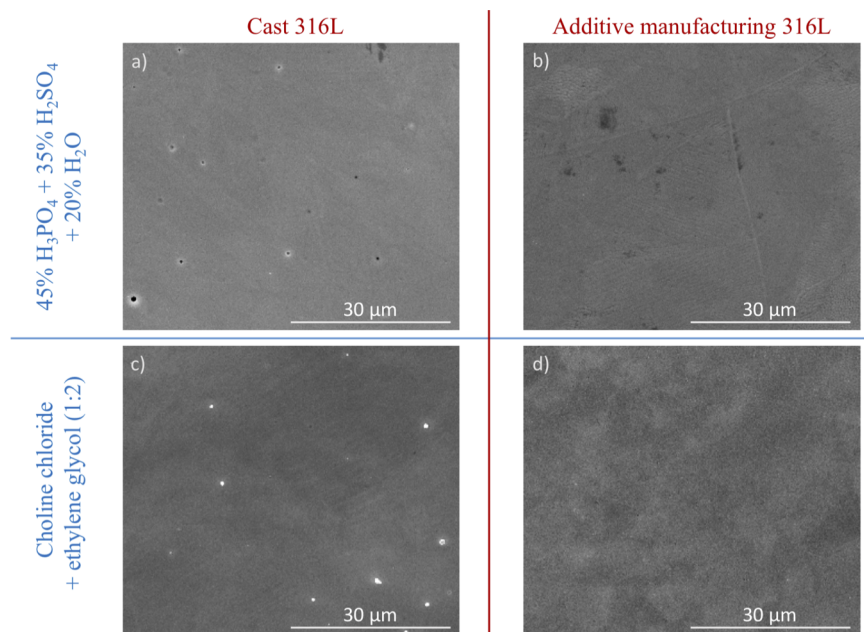


264

Figure 3: Levich's plot curves performed for cast and ALM 316L at  $2 \text{ mV s}^{-1}$  in ChCl-EG  
 265 (1:2) and acidic mixture at  $70^\circ\text{C}$

266 The manufacturing process used for the elaboration of materials is a pa-  
 267 rameter that strongly conditions the structural and functional properties of  
 268 the items. SEM observations of the sample after the EP procedure are pre-  
 269 sented in Fig. 4, showing a smooth surface. However, a preliminary study  
 270 has shown that for potentials corresponding to the zone of active dissolution,  
 271 the substrate is etched according to certain preferential plane (anisotropic  
 272 dissolution), whereas for a potential on the limiting-current plateau corre-  
 273 sponding to a diffusion control mechanism, a smooth and bright surface was  
 274 obtained for both samples and in both electrolytes without revealing the  
 275 microstructure. The area roughness parameters (arithmetical mean height)  
 276 determined by AFM measurements on  $10 \times 10 \mu\text{m}^2$  were between 1 and 2  
 277 nm for all the samples, with a maximum peak-to-valley height of 80 nm [12].

278



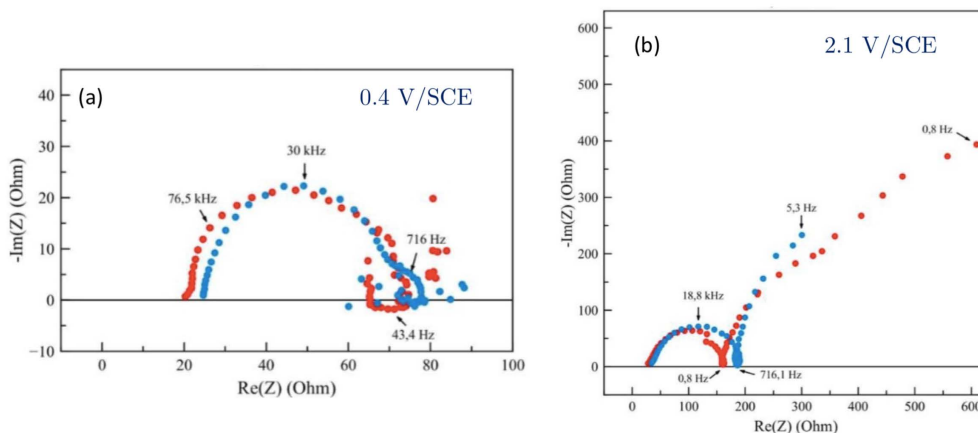
279

Figure 4: SEM observations of the samples after EP procedure at 70°C - 500 rpm. a) and  
 280 b) at 2.4 V/SCE, c) and d) at 3 V/SCE

281 EIS diagrams obtained for both materials in DES at 70°C are presented  
 282 in Fig. 5 for experiments performed at 0.4 V/SCE and 2.1 V/SCE. The EIS  
 283 response depends on the applied potential but is independent of the ma-  
 284 terials. Three time constants can be observed on these diagrams: a high  
 285 frequency capacitive semi-circle corresponding to the charge transfer resis-  
 286 tance in parallel with the capacitance of the interface, an inductive behavior  
 287 that may be ascribed either to the relaxation of adsorbed species or to the  
 288 relaxation of the thickness of corrosion-product layer with the potential, and  
 289 a low frequency time constant that can originate from diffusion process and  
 290 the relaxation of chemical steps. It should also be mentioned that the high  
 291 frequency domain shows a 45° slope that spreads over a larger frequency do-  
 292 main in DES (Fig. 5a) than in acidic solution (an example of EIS diagrams  
 293 in adic media is presented in Fig. 7), and that also depends on the applied  
 294 potential, thus indicating the formation of a porous layer which is thicker at

295 higher potential in DES (Fig. 5b).

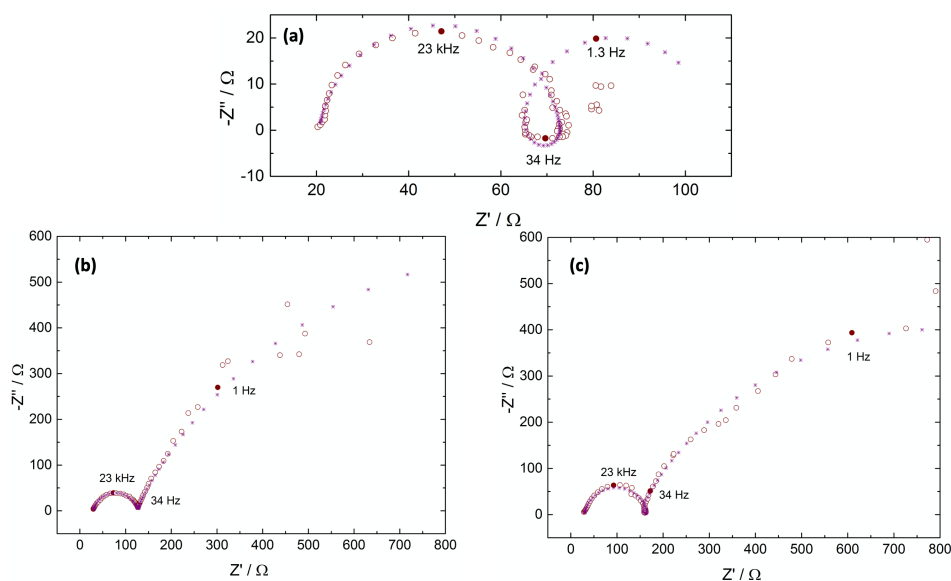
296



297

Figure 5: Experimental EIS diagrams for Cast (blue circles) and ALM (red circles) 316L  
298 SS electropolished in ChCl-EG at 70°C at 0.4 V/SCE (a) and 2.1 V/SCE (b)

299



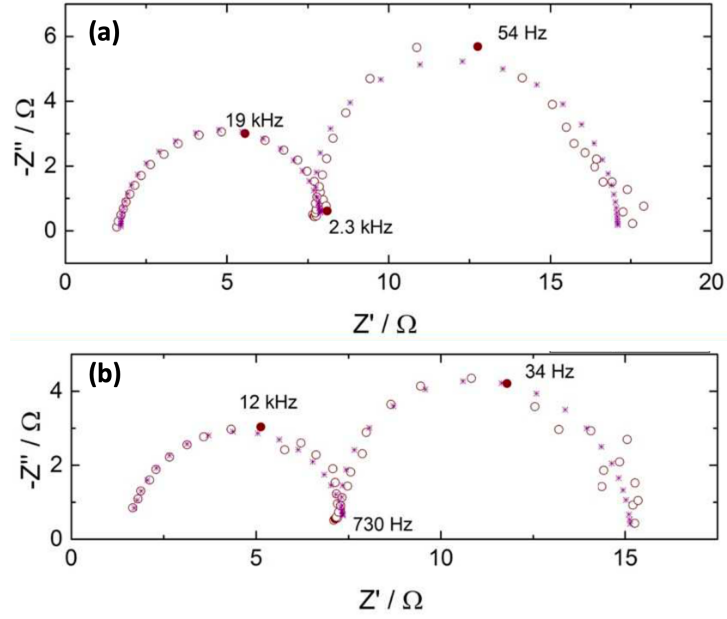
300

Figure 6: Experimental and calculated EIS diagrams for ALM 316L SS electropolished  
in ChCl-EG at 70°C at (a) 0.4 V/SCE; (b) 1.2 V/SCE; and (c) 2.1 V/SCE. Circles:  
301 experimental data; crosses: fit

302 Fig. 6 shows experimental and calculated EIS diagrams for ALM 316L SS  
303 electropolished in ChCl-EG at 70°C as a function of the potential. The low

304 frequency range was limited to the Hz domain since the response was noisy  
305 due to the evolution of the interface as a function of time. The two models  
306 in which either water or an acceptor specie is assumed to be the limiting  
307 specie were considered, but the comparison between fitting and experimen-  
308 tal results lead to the validation of the acceptor specie model, as shown with  
309 the fit results presented in Fig. 6. The fitted parameters presented in Ta-  
310 bles 3 and 4 show that the interfacial capacitance,  $C_{eff}$ , is systematically  
311 smaller than the value expected for a double layer capacitance (generally in  
312 the range of  $10 \mu\text{F cm}^2$ ), which indicates the formation of a thin layer of  
313 corrosion products (about 100-200 nanometers at 0.4 V/SCE) whose thick-  
314 ness increases with the polarization potential of the electrode. It was also  
315 observed that the electrolyte resistance, which is dependent on the system  
316 geometry and the conductivity of the solution, increases slightly with poten-  
317 tial. This variation can be explained in two ways: on the one hand by a  
318 variation in electrolyte conductivity due to the dissolution of material (the  
319 dissolution of the metal is accompanied by the consumption of ions of the  
320 solution, thus forming complexes), and on the other hand by a resistive con-  
321 tribution due to corrosion products on the electrode surface which is added  
322 to the resistance measured at high frequency. Theses variations for the elec-  
323 trolyte resistance and the interfacial capacitance are in agreement with the  
324 porous behavior of the electrode previously described in the high frequency  
325 domain. The desorption rate constant measured by the product  $K_d C_B$  (Ta-  
326 bles 3 and 4) tends towards a constant value when the potential increases,  
327 showing that this chemical step is a kinetic limitation in the EP process.  
328 The variations of the charge transfer resistance is also in agreement with the  
329 dissolution curve. It is higher on the plateau (smaller current) and larger on  
330 the active dissolution domain (i.e. a 0.4 V/SCE).

331



332

Figure 7: Experimental and calculated EIS diagrams for cast (a) and ALM 316L SS (b)  
 333 electropolished in acidic solution at 2.1 V/SCE. Circles: experimental data; crosses: fit

Table 3: Kinetic parameters obtained from the fitting procedure for the cast 316L in DES

Potential (V/SCE)	0.4	1.2	2.1
Interfacial capacitance $C_{eff}$ ( $\mu\text{F cm}^2$ )	$10.2 \pm 0.5$	$0.15 \pm 0.01$	$0.10 \pm 0.01$
Step 1 $K_1\alpha_1$	$(3 \pm 0.2) 10^{-1}$	$(4.3 \pm 0.3)$	$(5.9 \pm 0.3)$
Step 2 $K_2(\alpha_1 + \alpha_2)$	$(8.7 \pm 0.4) 10^{-5}$	$(4.3 \pm 0.2) 10^{-3}$	$(4.8 \pm 0.3) 10^{-3}$
Desorption step $K_d C_B$	$(3.4 \pm 0.2) 10^{-4}$	$(7 \pm 0.5) 10^{-4}$	$(6.9 \pm 0.5) 10^{-4}$

334 Interestingly, the same conclusions can be drawn for the analyses of the  
 335 EP treatments carried out in concentrated acid medium for both materials as  
 336 shown for the EIS diagrams presented in Fig. 7. The shape of the impedance  
 337 diagrams is very similar to the one obtained in DES at the same potential ( $E$   
 338  $= 2.1$  V/SCE), but the two low-frequency time constants, namely the induc-  
 339 tive time constant the kHz range and the capacitive time constant around the  
 340 tenth of Hz, are shifted towards higher frequency domain when the polishing  
 341 was performed in aqueous solution. These experimental data were analyzed

Table 4: Kinetic parameters obtained from the fitting procedure for the ALM 316L in DES

Potential (V/SCE)	0.4	1.2	2.1
Interfacial capacitance $C_{eff}$ ( $\mu\text{F cm}^2$ )	$0.20 \pm 0.01$	$0.12 \pm 0.01$	$0.10 \pm 0.01$
Step 1 $K_1\alpha_1$	$(4.5 \pm 0.2) 10^{-2}$	$(3.0 \pm 0.2)$	$(6.1 \pm 0.7)$
Step 2 $K_2(\alpha_1 + \alpha_2)$	$(5.4 \pm 0.3) 10^{-4}$	$(9.9 \pm 0.3) 10^{-4}$	$(9.3 \pm 0.4) 10^{-5}$
Desorption step $K_dC_B$	$(3.2 \pm 0.1) 10^{-5}$	$(3.2 \pm 0.2) 10^{-3}$	$(3.2 \pm 0.2) 10^{-3}$

342 using the same model than the one used for the analysis of results obtained  
343 in DES and the fitted parameters are presented in Tables 5. The value of  
344 the interfacial capacitance (larger than  $1 \mu\text{F cm}^2$ ) is significantly higher than  
345 in the case of an EP in the DES, which is consistent with either a double  
346 layer capacitance for a metal/electrolyte interface in highly concentrated so-  
347 lution, or with a combination in series of a capacitance ascribed to a very  
348 thin corrosion product layer in series with the double layer capacitance. It is  
349 therefore deduced that the proposed mechanism makes it possible to account  
350 for electropolishing in the most commonly used media (acid solutions) but  
351 also in new solvents which are increasingly used because of their eco-friendly  
352 nature.

Table 5: Kinetic parameters obtained from the fitting procedure for the cast and ALM 316L in acidic electrolyte at 2.1 V/SCE

	Cast 316L	ALM 316L
Interfacial capacitance $C_{eff}$ ( $\mu\text{F cm}^2$ )	$1.10 \pm 0.04$	$1.90 \pm 0.06$
Step 1 $K_1\alpha_1$	$(7.9 \pm 0.4) 10^2$	$(4.2 \pm 0.3) 10^2$
Step 2 $K_2(\alpha_1 + \alpha_2)$	$(7.7 \pm 0.5) 10^{-4}$	$(1.7 \pm 0.2) 10^{-4}$
Desorption step $K_dC_B$	$(1.2 \pm 0.1) 10^{-6}$	$(2.7 \pm 0.1) 10^{-6}$

353 **5. Conclusions**

354 This study has showed with the analysis of the experimental electro-  
355 chemical impedance diagrams that the model involving an acceptor specie  
356 enables to describe all the results obtained for the two materials, namely  
357 the cast 316L and the ALM 316L. The proposed mechanism makes it possi-  
358 ble to describe, from a kinetic point a view, the electropolishing process for  
359 concentrated acidic media and DES. However, as the number of variables  
360 is large and since they depend on each other, only combinations of these  
361 parameters can be obtained from the analysis of impedance spectra and the  
362 fitting procedure. It should be noted, however, that the value of the inter-  
363 facial capacitance measured in the case of electropolishing in DES can be  
364 linked to the formation of a corrosion product thin film, which also results  
365 in a slight increase of the electrolyte resistance.

366 **Acknowledgements**

367 Chloé Rotty gratefully acknowledges financial support from the program  
368 "MoMeQa Innovation Stratégique Industrielle ISI" and BPI France. The  
369 authors are grateful to Mr. N. Rouge, PCU UTINAM platform for his help  
370 on SEM images.

371 **References**

- 372 [1] W. E. Frazier, Metal additive manufacturing: A review, *Journal*  
373 *of Materials Engineering and Performance* 23 (6) (2014) 1917–1928.  
374 doi:10.1007/s11665-014-0958-z.
- 375 [2] S. M. Thompson, L. Bian, N. Shamsaei, A. Yadollahi, An overview  
376 of direct laser deposition for additive manufacturing; part i: Transport  
377 phenomena, modeling and diagnostics, *Additive Manufacturing* 8 (2015)  
378 36–62. doi:10.1016/j.addma.2015.07.001.
- 379 [3] N. Shamsaei, A. Yadollahi, L. Bian, S. M. Thompson, An overview of  
380 direct laser deposition for additive manufacturing; part ii: Mechanical  
381 behavior, process parameter optimization and control, *Additive Manu-*  
382 *facturing* 8 (2015) 12–35. doi:10.1016/j.addma.2015.07.002.
- 383 [4] A. K. Au, W. Huynh, L. F. Horowitz, A. Folch, 3d-printed microfluidics,  
384 *Angewandte Chemie - International Edition* 55 (12) (2016) 3862–3881.  
385 doi:10.1002/anie.201504382.
- 386 [5] E. O. Olakanmi, R. F. Cochrane, K. W. Dalgarno, A review on selective  
387 laser sintering/melting (sls/slm) of aluminium alloy powders: Process-  
388 ing, microstructure, and properties, *Progress in Materials Science* 74  
389 (2015) 401–477. doi:10.1016/j.pmatsci.2015.03.002.
- 390 [6] J. H. Tan, W. L. E. Wong, K. W. Dalgarno, An overview of powder  
391 granulometry on feedstock and part performance in the selec-  
392 tive laser melting process, *Additive Manufacturing* 18 (2017) 228–255.  
393 doi:10.1016/j.addma.2017.10.011.
- 394 [7] J. L. Bartlett, X. Li, An overview of residual stresses in metal  
395 powder bed fusion, *Additive Manufacturing* 27 (2019) 131–149.  
396 doi:10.1016/j.addma.2019.02.020.
- 397 [8] D. Landolt, Fundamental aspects of electropolishing, *Electrochim-*  
398 *ica Acta* 32 (1) (1987) 1 – 11. doi:https://doi.org/10.1016/0013-  
399 4686(87)87001-9.

- 400 [9] W. Han, F. Fang, Fundamental aspects and recent developments in elec-  
401 tropolishing, *International Journal of Machine Tools and Manufacture*  
402 139 (2019) 1 – 23. doi:10.1016/j.ijmachtools.2019.01.001.
- 403 [10] A. P. Abbott, G. Capper, K. J. McKenzie, A. Glidle, K. S. Ryder, Elec-  
404 tropolishing of stainless steels in a choline chloride based ionic liquid:  
405 an electrochemical study with surface characterisation using sem and  
406 atomic force microscopy, *Phys. Chem. Chem. Phys.* 8 (2006) 4214–4221.  
407 doi:10.1039/B607763N.
- 408 [11] C. Rotty, M.-L. Doche, A. Mandroyan, J.-Y. Hihn, Electropolish-  
409 ing behavior of additive layer manufacturing 316l stainless steel in  
410 deep eutectic solvents, *ECS Transactions* 77 (11) (2017) 1199–1207.  
411 doi:10.1149/07711.1199ecst.
- 412 [12] C. Rotty, A. Mandroyan, M.-L. Doche, S. Monney, J.-Y. Hihn,  
413 N. Rouge, Electrochemical superfinishing of cast and alm 316l stain-  
414 less steels in deep eutectic solvents: Surface microroughness evolution  
415 and corrosion resistance, *Journal of the Electrochemical Society* 166 (13)  
416 (2019) C468–C478. doi:10.1149/2.1211913jes.
- 417 [13] W. Han, F. Fang, Two-step electropolishing of 316l stainless steel in a  
418 sulfuric acid-free electrolyte, *Journal of Materials Processing Technology*  
419 279 (2020) 116558. doi:10.1016/j.jmatprotec.2019.116558.
- 420 [14] A. Awad, N. A. Ghany, T. Dahy, Removal of tarnishing and roughness  
421 of copper surface by electropolishing treatment, *Applied Surface Science*  
422 256 (13) (2010) 4370 – 4375. doi:10.1016/j.apsusc.2010.02.033.
- 423 [15] C. A. Huang, J. H. Chang, W. J. Zhao, S. Y. Huang, Examination  
424 of the electropolishing behaviour of 73 brass in a 70rotating disc elec-  
425 trode, *Materials Chemistry and Physics* 146 (3) (2014) 230 – 239.  
426 doi:10.1016/j.matchemphys.2014.02.052.
- 427 [16] C. Rotty, A. Mandroyan, M.-L. Doche, J. Hihn, Electropolishing of  
428 cuzn brasses and 316l stainless steels: Influence of alloy composition or  
429 preparation process (alm vs. standard method), *Surface and Coatings*  
430 *Technology* 307 (2016) 125 – 135. doi:10.1016/j.surfcoat.2016.08.076.

- 431 [17] R. Sautebin, H. Froidevaux, D. Landolt, Theoretical and experimental  
432 modeling of surface leveling in ECM under primary current distribution  
433 conditions, *Journal of The Electrochemical Society* 127 (5) (1980) 1096.  
434 doi:10.1149/1.2129823.
- 435 [18] R. Sautebin, D. Landolt, Anodic leveling under secondary and tertiary  
436 current distribution conditions, *Journal of The Electrochemical Society*  
437 129 (5) (1982) 946. doi:10.1149/1.2124071.
- 438 [19] C. Clerc, D. Landolt, On the theory of anodic levelling: Fem simulation  
439 of the influence of profile shape and cell geometry, *Electrochimica Acta*  
440 29 (6) (1984) 787 – 795. doi:10.1016/0013-4686(84)80015-8.
- 441 [20] P. Jacquet, A new method of achieving perfectly polished metallic sur-  
442 faces, *Comptes Rendus Hebdomadaires des Seances de l'Academie des*  
443 *Sciences* 201 (1935) 1473–1475.
- 444 [21] P. Jacquet, Regarding the electrolytic polishing of aluminum, *Comptes*  
445 *Rendus Hebdomadaires des Seances de l'Academie des Sciences* 205  
446 (1937) 1232–1235.
- 447 [22] W. Elmore, Electrolytic polishing, *Journal of Applied Physics* 10 (10)  
448 (1939) 724–727. doi:10.1063/1.1707257.
- 449 [23] W. Elmore, Electrolytic polishing II, *Journal of Applied Physics* 11 (12)  
450 (1940) 797–799. doi:10.1063/1.1712738.
- 451 [24] C. Wagner, Contribution to the theory of electropolishing, *Journal of*  
452 *The Electrochemical Society* 101 (5) (1954) 225. doi:10.1149/1.2781235.
- 453 [25] J. Edwards, The mechanism of electropolishing of copper in phosphoric  
454 acid solutions, *Journal of The Electrochemical Society* 100 (8) (1953)  
455 223C. doi:10.1149/1.2781129.
- 456 [26] J. Edwards, The mechanism of electropolishing of copper in phosphoric  
457 acid solutions, *Journal of The Electrochemical Society* 100 (7) (1953)  
458 189C. doi:10.1149/1.2781122.

- 459 [27] M. Matloz, Modeling of impedance mechanisms in electropolish-  
460 ing, *Electrochimica Acta* 40 (4) (1995) 393–401. doi:10.1016/0013-  
461 4686(94)00287-B.
- 462 [28] M. Bojinov, I. Betova, G. Fabricius, T. Laitinen, R. Raicheff, Passi-  
463 vation mechanism of iron in concentrated phosphoric acid, *Journal of*  
464 *Electroanalytical Chemistry* 475 (1) (1999) 58–65. doi:10.1016/S0022-  
465 0728(99)00343-5.
- 466 [29] O. E. Barcia, O. R. Mattos, B. Tribollet, , *Journal of The Electrochem-*  
467 *ical Society* 139 (2) (1992) 446. doi:10.1149/1.2069238.  
468 URL
- 469 [30] I. Epelboin, M. Keddam, J. C. Lestrade, Faradaic impedances and in-  
470 termediates in electrochemical reactions, *Faraday Discuss. Chem. Soc.*  
471 56 (1973) 264–275. doi:10.1039/DC9735600264.
- 472 [31] I. Epelboin, M. Keddam, O. Mattos, H. Takenouti, The dissolution and  
473 passivation of fe and fe-cr alloys in acidified sulphate medium: Influences  
474 of ph and cr content, *Corrosion Science* 19 (7) (1979) 1105 – 1112.  
475 doi:10.1016/S0010-938X(79)80099-2.
- 476 [32] C. Cachet, F. Ganne, G. Maurin, J. Petitjean, V. Vivier, R. Wiart, EIS  
477 investigation of zinc dissolution in aerated sulfate medium. Part I: bulk  
478 zinc, *Electrochimica Acta* 47 (3) (2001) 509–518. doi:10.1016/S0013-  
479 4686(01)00740-X.
- 480 [33] M. P. Gomes, I. Costa, N. Pébère, J. L. Rossi, B. Tribollet, V. Vivier,  
481 On the corrosion mechanism of mg investigated by electrochemical  
482 impedance spectroscopy, *Electrochimica Acta* 306 (2019) 61 – 70.  
483 doi:10.1016/j.electacta.2019.03.080.
- 484 [34] M. E. Orazem, B. Tribollet, *Electrochemical Impedance Spectroscopy,*  
485 2nd Edition, The ECS Series of Texts and Monographs, Wiley, Hoboken,  
486 NJ, 2017.
- 487 [35] I. D. Raistrick, J. R. Macdonald, D. R. Franceschetti, *Theory in*

- 488 *Impedance Spectroscopy*, John Wiley & Sons, Ltd, 2018, Ch. 2, pp.  
489 21–105. doi:10.1002/9781119381860.ch2.
- 490 [36] W. Watson, M. E. Orazem, EIS: Measurement model program (Sep  
491 2020).  
492 URL [ecsarxiv.org/kze9x](https://ecsarxiv.org/kze9x)
- 493 [37] H. Liao, W. Watson, A. Dizon, B. Tribollet, V. Vivier, M. E.  
494 Orazem, Physical properties obtained from measurement model analy-  
495 sis of impedance measurements, *Electrochimica Acta* 354 (2020) 136747.  
496 doi:10.1016/j.electacta.2020.136747.

497 **List of Symbols**

- 498 –  $C_{dl}$ : double layer capacitance (in  $\mu\text{F cm}^2$ )
- 499 –  $C_{eff}$ : interfacial capacitance (in  $\mu\text{F cm}^2$ )
- 500 –  $C_s$ : concentration of the species  $s$  (in  $\text{mol L}^{-1}$ )
- 501 –  $D_s$ : diffusion coefficient of the species  $s$  (in  $\text{cm}^2 \text{s}^{-1}$ )
- 502 –  $E$ : Electrode potential (in V)
- 503 –  $f$ : frequency (in Hz)
- 504 –  $F$ : Faraday's constant ( $96485 \text{ C mol}^{-1}$ )
- 505 –  $i$ : current density (in  $\text{A cm}^{-2}$ )
- 506 –  $k_i$ : kinetic constant of reaction  $i$  linked to  $K_i$  via Eq. (3) (in  $\text{cm}^{-2} \text{s}^{-1}$ )
- 507 –  $K_i$ : kinetic constant of reaction  $i$  (in  $\text{cm}^{-2} \text{s}^{-1}$ )
- 508 –  $p$ : variable in the Laplace domain
- 509 –  $Q_{int}$ : constant-phase-element parameter (in  $\text{F/s}^{(1-\alpha_{int})} \text{ cm}^2$ )
- 510 –  $r$ : radius of the electrode (in cm)
- 511 –  $R$ : gas constant ( $8.314 \text{ J K}^{-1} \text{ mol}^{-1}$ )
- 512 –  $R_{el}$ : electrolyte resistance (in  $\Omega \text{ cm}^2$ )
- 513 –  $T$ : temperature (in K)
- 514 –  $v_i$ : rate of the reaction  $i$
- 515 –  $Y$ : admittance (in  $\text{S cm}^{-2}$ )
- 516 –  $Z$ : impedance (in  $\Omega \text{ cm}^2$ )
- 517 –  $Z_f$ : faradaic impedance (in  $\Omega \text{ cm}^2$ )
- 518 –  $\alpha_i$ : charge transfer coefficient of reaction  $i$
- 519 –  $\alpha_{int}$ : constant-phase-element parameter

- 520    –  $\beta$ : surface concentration for complete coverage (in mol cm<sup>-2</sup>)
- 521    –  $\eta$ : dynamic viscosity (in Pa s)
- 522    –  $\nu$ : kinematic viscosity (in cm<sup>2</sup> s<sup>-1</sup>)
- 523    –  $\rho$ : density (in g cm<sup>-3</sup>)
- 524    –  $\sigma$ : conductivity (in S cm<sup>-1</sup>)
- 525    –  $\theta_1$ : surface coverage of  $MA_{ads}^+$
- 526    –  $\theta_2$ : surface coverage of  $MA_{ads}^{2+}$
- 527    –  $\omega$ : angular frequency (in rad s<sup>-1</sup>)
- 528    –  $\Omega$ : rotation rate of the RDE (in rad s<sup>-1</sup>)

529 **List of Figures**

530	1	Electrical equivalent circuit used to analyse the EIS spectra. $Z_f$ allows to introduce the analytical expression of the impedance that is derived from the electropolishing model presented in this work. . . . .	11
531			
532			
533			
534	2	Polarization curves obtained for cast and ALM 316L at 2 mV s <sup>-1</sup> and $\Omega= 500$ rpm in acidic mixture (a) and in ChCl-EG (1:2) at 70°C (b) . . . . .	13
535			
536			
537	3	Levich's plot curves performed for cast and ALM 316L at 2 mV s <sup>-1</sup> in ChCl-EG (1:2) and acidic mixture at 70°C . . . .	14
538			
539	4	SEM observations of the samples after EP procedure at 70°C - 500 rpm. a) and b) at 2.4 V/SCE, c) and d) at 3 V/SCE . .	15
540			
541	5	Experimental EIS diagrams for Cast (blue circles) and ALM (red circles) 316L SS electropolished in ChCl-EG at 70°C at 0.4 V/SCE (a) and 2.1 V/SCE (b) . . . . .	16
542			
543			
544	6	Experimental and calculated EIS diagrams for ALM 316L SS electropolished in ChCl-EG at 70°C at (a) 0.4 V/SCE; (b) 1.2 V/SCE; and (c) 2.1 V/SCE. Circles: experimental data; crosses: fit . . . . .	16
545			
546			
547			
548	7	Experimental and calculated EIS diagrams for cast (a) and ALM 316L SS (b) electropolished in acidic solution at 2.1 V/SCE. Circles: experimental data; crosses: fit . . . . .	18
549			
550			